First-principles DFT+DMFT calculations of structural properties of actinides: Role of Hund's exchange, spin-orbit coupling, and crystal structure

Bernard Amadon*
CEA, DAM, DIF, F-91297 Arpajon, France

(Received 24 February 2016; revised manuscript received 26 August 2016; published 22 September 2016)

We utilize a combination of an *ab initio* calculation of effective Coulomb interactions and a DFT+DMFT calculation of total energy to study the structural properties of pure actinides. We first show that the effective direct Coulomb interactions in plutonium and americium are much smaller than usually expected. Secondly, we emphasize the key role of Hund's exchange in combination with the spin-orbit coupling in determining the structural parameters of δ-plutonium and americium. Thirdly, using this *ab initio* description, we reproduce the experimental transition from low volume early actinides (uranium, neptunium, α-plutonium) to high-volume late actinides (δ-plutonium, americium, and curium) without the need of an artificial magnetism. Finally, we compare the energies and structural properties of α, γ, ϵ, and δ phases of plutonium to experimental data.

DOI: 10.1103/PhysRevB.94.115148

I. INTRODUCTION

The structural properties of pure actinides behave uniquely in the periodic table: as the atomic number increases, the volume exhibits a jump [1,2]. This is qualitatively understood as being the result of the competition between chemical bonding and Coulomb interaction. Indeed, lighter elements, including α-uranium, α-neptunium, and α-plutonium, are usually described as containing delocalized electrons. Thus their volumes are low. In these systems, indeed, chemical bonding between $5f$ orbitals is expected to be strong [1], explaining the low symmetry of these phases and their low volumes. Starting with americium, the volumes are high (see Fig. 3); electron correlation is stronger than chemical bonding therefore making the crystal structure more compact. Plutonium is peculiar because it is at the verge of localization [1], as shown by the large number of phases with different volumes, crystallographic structures, and physical properties. In particular, the δ phase, stable only at 600 K, has a large volume. In contrast to actinides, lanthanides [3], because of their localized $4f$ orbitals, are much simpler and contain localized electrons that do not participate to the bonding, thus their equilibrium volumes are large (see, e.g., Refs. [4,5]).

In order to describe the existence of phases with various degrees of electron localization, a single formalism able to describe localized and delocalized phases is needed. However, density functional theory, with the available density functionals, needs an artificial [6] spin and/or orbital moment in order to increase the localization of electrons and describe the large equilibrium volumes of localized phases such as plutonium [2,7–9], americium [10,11], or the structures of actinides [12]. Without magnetism, DFT/GGA only describes localized phases as delocalized [2]. Other methods were designed to describe phases in which the interaction between electrons leads to localization. Indeed, the self-interaction correction method [13], hybrid functionals, or the DFT+U approach have been able to describe some localized phases of actinides [14–16] or lanthanides [17,18].

A coherent description of spectroscopic, magnetic, and structural properties of strongly correlated systems was obtained in the last 15 years with the combination of density functional theory and dynamical mean-field theory (DFT+DMFT) [19]. In particular, the physics of plutonium has triggered a large number of theoretical studies [20–31] but only a few of them focused on structural properties: Savrasov *et al.* [20] showed that the α-δ transition in plutonium can be described using DFT+DMFT, and that the main physical picture can be reproduced by an isostructural transition like in cerium metal. However, this pioneering calculation had to use many simplifications. Later, the Gutzwiller approximation was used [32] to show the importance of the atomic structure. These calculations, and others [24,26,33], however, relied on values of effective interactions, taken as *ad hoc* parameters. Moreover, because a unified *ab initio* description of actinide structural and magnetic properties is lacking, the relative roles of electronic interactions, crystallographic structure, and relativistic effects are not understood in the actinide series.

Here, we carry out a self-consistent calculation of the effective interaction [34–37] and show that the direct Coulomb term is weak, even for plutonium and americium. Using these interactions, we use DFT+DMFT to study the structural properties and the relative stability of phases. We find that—for elements that are at the verge of localization, such as plutonium, and americium—structural properties are indeed driven by the combination of Hund's exchange [38] and spin-orbit coupling.

Sections II, III, and IV, respectively, present the methods, the effective interaction results, and the DFT+DMFT calculations of the structural properties. Appendix A estimates the uncertainty on the value of our effective interactions. Appendix B presents the spectral functions of actinides as computed by DFT+DMFT.

II. METHODS AND COMPUTATIONAL DETAILS

Our computational scheme is summarized in Fig. 1. All our calculations use the projector augmented wave [43] (PAW) framework [44] and use a modified version of the open source code ABINIT [45]. Details about atomic data validation are given in Ref. [46], Sec. I.

We first compute the effective direct Coulomb interaction U and Hund interactions J with our self-consistent DFT+U

*bernard.amadon@cea.fr

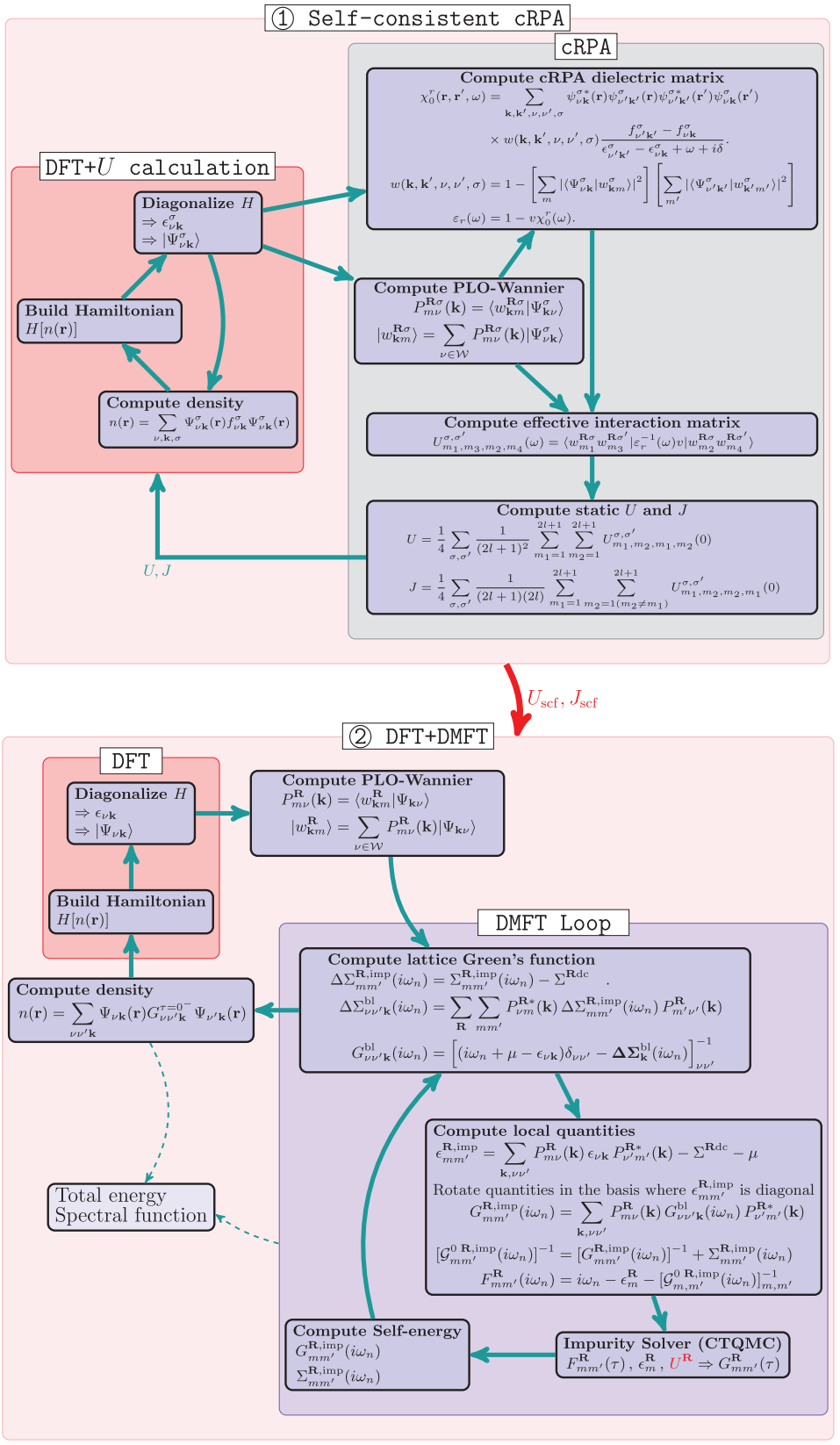

FIG. 1. Calculation scheme used in this study. The first part of the calculation is a self-consistent cRPA scheme as implemented by us and discussed in Ref. [37] and in Sec. II A. The self-consistent values of U and J are used in a fully self-consistent DFT+DMFT calculation as implemented by us in ABINIT [39] using the same Wannier functions [39,40], and a continuous time quantum Monte Carlo solver [41] to solve the Anderson impurity model. At full self-consistency, the total internal energy is computed following Refs. [39,42], and the f spectral function is computed using the maximum entropy method (see also text). Notations in this scheme are the same as in Refs. [37,39,40].

implementation [37] of the constrained random phase approximation (cRPA) [34]. We use then our implementation of DFT+DMFT as in Refs. [39,41,47] to compute the total energy. Such scheme is a way to carry out parameter-free DFT+DMFT calculations. This is a simplification of the more general parameter-free combination [48–56] of the GW approximation and the DMFT scheme, for which the effective interaction is also self-consistently computed. Nevertheless, in GW+DMFT, the screening takes into account the full DFT+DMFT response function and the dynamical nature of the interaction is taken into account. However, this method is still under development by several groups, and computing the total energy in GW+DMFT is still a formidable task.

Here, the self-consistency loop to determine U is carried out within DFT+U. This scheme [35] has been used some time before to compute the effective interactions in gadolinium [35], NiO [35,36], $CuGaS_2$ [36], transition-metal oxides [36], as well as cerium and UO_2 [37]. More generally, to our knowledge, no calculation (self-consistent or not) has been devoted to pure actinides. Here, we thus apply the self-consistent method to compute U in pure actinides from uranium to curium.

Then, fully self-consistent DFT+DMFT—able to deal with localized/delocalized transition (see, e.g., Ref. [41])—is used to compute the total energy. Early DFT+DMFT calculations of total energy were scarce, because of the computational cost, and pioneering calculations have to make some necessary approximations, such as the use of an approximate solver [20,22,39,57–59] or the lack of self-consistency on the density [42,60–65]. However, with the advent of efficient solvers [66,67] for the Anderson impurity model and the development of supercomputers, precise calculations of total energy using continuous-time quantum Monte Carlo (CTQMC) solvers and full self-consistency over electronic density appeared [41,68–76]. Among them, and because of the computational challenge to study systems with high degeneracy, only a few of these studies focused on f-electron systems [41,76] and none focused on actinides. Here we compute the total energy of pseudo-α-U, α-Np, α-Pu, γ-Pu, ϵ-Pu, δ-Pu, Am, and Cm with self-consistent DFT+DMFT solved with a CTQMC solver [41,45]. In the following section, we discuss technical details of the constrained random phase approximation and then the DFT+DMFT.

A. Calculation of effective interactions

1. Self-consistent cRPA calculation

We use our self-consistent [35] DFT+U implementation [37] of the constrained random phase approximation [34] in order to compute the effective direct Coulomb interaction U and Hund's interactions J for actinides. The scheme is detailed in Ref. [37] and sketched in the top of Fig. 1. First a standard DFT+U calculation is converged (with an arbitrary value of U). Wave functions $\Psi^{\sigma}_{\nu\mathbf{k}}$ and eigenvalues $\epsilon^{\sigma}_{\nu\mathbf{k}}$ are used to compute the constrained noninteracting polarizability χ_0. To do this, the transitions among correlated orbitals are removed through a weighting scheme (involving the function w, which depends on correlated Wannier orbitals $w^{\mathbf{R}\sigma}_{\mathbf{k}m}$) as described in Fig. 1 and in Refs. [36,37]. The effective interaction matrix U is then computed by projecting the cRPA interaction on projected local orbital Wannier functions for correlated orbitals as discussed extensively in Ref. [37]. Then the static effective interactions are used in another DFT+U calculation until full self-consistency is reached on U and J.

2. Computational details

We use a 4×4×4 k-point grid, and energy cutoffs for the wave functions, the dielectric function and the bare Coulomb interaction are respectively 20, 10, and 60 Ha. Sixty bands are sufficient for the calculation of the polarizability. For simplicity (and only for the cRPA calculation), the fcc phase was used for all actinides, and spin-orbit coupling was neglected. We carefully checked the dependency of the energy window and we find a small increase of U if more bands are used to define Wannier functions in agreement with our previous results on cerium [37]. Concerning the calculation on iron discussed below, we used 11 Kohn Sham bands to define the energy window, and carefully converged the energy cutoffs and the k-point mesh.

B. DFT+DMFT

1. Correlated orbital, self-consistency

We briefly remind the basic step of our DFT+DMFT scheme [39,40,45] in the bottom of Fig. 1, using the notations of Refs. [39,40]: first we carry out a DFT calculation. We use the GGA [77] approximation for DFT as proposed by Söderlind *et al.* [78] to describe actinides. Then, we use Kohn-Sham eigenvalues $\epsilon_{\nu\mathbf{k}}$ to build the Bloch (bl) lattice Green's function $G^{\mathrm{bl}}_{\nu\nu'\mathbf{k}}$. Kohn-Sham eigenvectors $|\Psi_{\nu\mathbf{k}}\rangle$ are used to define correlated orbitals as Wannier functions [40] $|w^{\mathbf{R}\sigma}_{\mathbf{k}m}\rangle$. As in Ref. [47], we take into account the spin-orbit coupling and we use an energy window with 26 Kohn-Sham states per atom (without the semicore states) to built the $5f$ Wannier functions. Then the local Green's function is computed, from which the hybridization function is obtained. The impurity model is solved using CTQMC (see next section), from which the self-energy is deduced and then the full Green's function is recomputed until self-consistency over the local Green's function is achieved. Then the density is recomputed to update the DFT Hamiltonian as in Refs. [39,41]. In practice, however, it is much more efficient to update simultaneously the density and the local Green's function, as discussed in Ref. [45]. The full localized limit double counting is used as in Ref. [39].

2. CTQMC solver

We use our recent implementation [41] of the CTQMC [66] solver in the density-density approximation (see Ref. [46], Sec. II), as available in ABINIT [45]. This approximation offers a good compromise between computational cost and precision. The results of our calculation suggest that this approach is sufficient to describe structural properties. As spin-orbit coupling is taken into account in DFT+DMFT calculations, we take into account off-diagonal hybridization in the Monte Carlo calculation. There are no noticeable sign problems. We use between 5×10^7 and 10^9 Monte Carlo steps—depending on the system studied—in order that the DFT+DMFT total energy is converged to less than 0.5 meV.

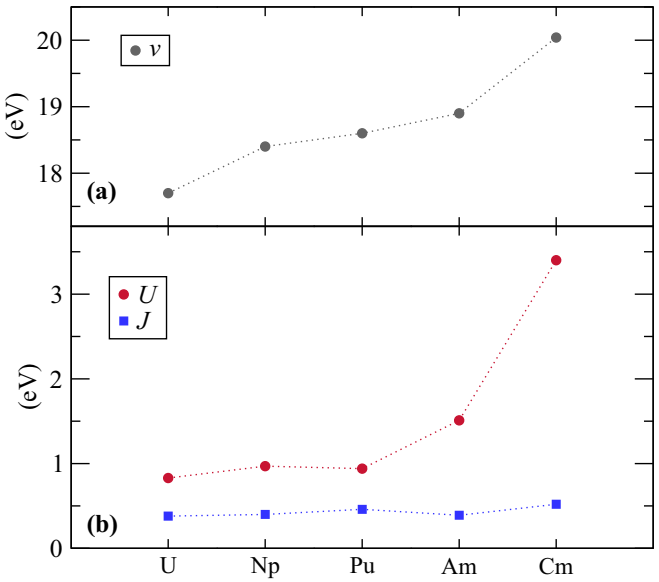

FIG. 2. *Ab initio* bare and effective interactions in actinides. Bare direct Coulomb interaction v [on part (a)], Hubbard U, and Hund exchange J [on part (b)] interactions for U, Np, Pu, Am, and Cm.

3. Total energy and structure

Our DFT+DMFT calculations are done at 800 and 200 K, and for the studied systems, equilibrium volumes are mainly insensitive to this variation of temperature. For all phases, we use the experimental internal parameters, only the volume is relaxed and we focus on the paramagnetic phase, which is the stable phase at room temperature. Uranium, neptunium, plutonium [6], and americium [1] have no local magnetic moment, so electronic entropy is expected to be weak and thus neglected. For curium, entropy should probably be taken into account for a more precise determination of the structural properties, but it is not the goal of this study. For α-plutonium, we used the pseudo α phase, proposed by Bouchet *et al.* [79], but calculations on the α phase are also performed as a check (see Ref. [46], Sec. III). See also Ref. [46], Sec I, for some other computational details.

III. CALCULATION OF EFFECTIVE INTERACTIONS IN ACTINIDES

Results

The values for effective direct interactions, given in Fig. 2 and Table I, are surprisingly much smaller—$\simeq$ 1 eV for plutonium—than the value of $\simeq$4 eV previously assumed, e.g., for plutonium and americium [20,24,26,30–32]. In comparison, we have computed the value of U in cerium and iron, and we found respectively 5.5 eV [37] for cerium—in agreement with Ref. [89]—and 1.62 eV for iron in agreement with the value of 1.4 eV obtained in Ref. [90] with the same scheme.[1] It is thus another validation of our computational scheme to determine U. Two reasons explain the low values obtained in actinides. First, the bare interaction (see Fig. 2 and Table I) is lower for $5f$ orbitals in comparison to $4f$ orbitals (24 eV for cerium [37]) and $3d$ orbitals (22.9 eV for iron[2]). Secondly, the screening due to transitions between f orbitals and noncorrelated orbitals is important in actinides, because f orbitals are near the Fermi level, as in iron but in contrast to cerium [37]. However, coherently to what is observed in lanthanides, the effective interaction U in curium is more important because f orbitals are far from the Fermi level [24,91].[3] Lastly, it is interesting to notice in Fig. 2 that uranium and plutonium have nearly the same interactions U and J in contrast to the usual values assumed in the literature [20,92].

TABLE I. Value in eV of effective and bare interactions for actinides. U^{crpa} is the F^0 Slater integral and $U^{\mathrm{crpa}}_{\mathrm{diag}}$ is the average of the diagonal elements of the direct Coulomb interaction matrix (see, e.g., Ref. [37]).

	U	Np	Pu	Am	Cm
U^{crpa}	0.8	1.0	0.95	1.5	3.4
$U^{\mathrm{crpa}}_{\mathrm{diag}}$	1.5	1.7	1.7	2.3	4.3
J^{crpa}	0.4	0.4	0.45	0.4	0.55
U^{bare}	17.7	18.4	18.6	18.9	20.0
J^{bare}	0.55	0.55	0.6	0.55	0.6

Concerning Hund's exchange, Fig. 2 shows that it is nearly constant for all actinides: it highlights the fact that the Hund's exchange is not efficiently screened [93]. We will see below that Hund's exchange is the most important mechanism driving the structural properties.

IV. DFT+DMFT CALCULATIONS OF STRUCTURAL PROPERTIES OF ACTINIDES: RESULTS

A. Results and discussion

We carried out DFT+DMFT calculations, using these *ab initio* interaction parameters. Figure 3 and Table II compares our DFT+DMFT theoretical equilibrium volumes and bulk moduli with experiment and other calculations. First, it shows [see Fig. 3(d)] that the combination of DFT+DMFT and an *ab initio* calculation of interaction parameters describes correctly the structural parameters in actinides without the need for an artificial ordered magnetism. We will now discuss the results in more details.

1. α-U, α-Np, and α-Pu

We first discuss early actinides. For α-U, α-Np, and α-Pu, the GGA/PBE approximation gives reasonable agreement with experiment. So the need for more advanced theories is less stringent than for the phases of plutonium, americium, and

[1]Note that for iron, in order to compare with literature, we give the non-self-consistent value. Besides, the average U_{diag} of diagonal elements of the direct Coulomb interaction matrix is sometimes used in the literature instead of the F^0 Slater integral. We found that $U_{\mathrm{diag}} = 2.8$ eV, whereas Shih *et al.* find 2.4 eV.

[2]Our value for the average of the diagonal bare interaction is 24.3 eV, whereas Shih *et al.* find 22.5 eV

[3]Our DFT+U density of states is rather similar to the spectral functions obtained by Gouder *et al.* [91].

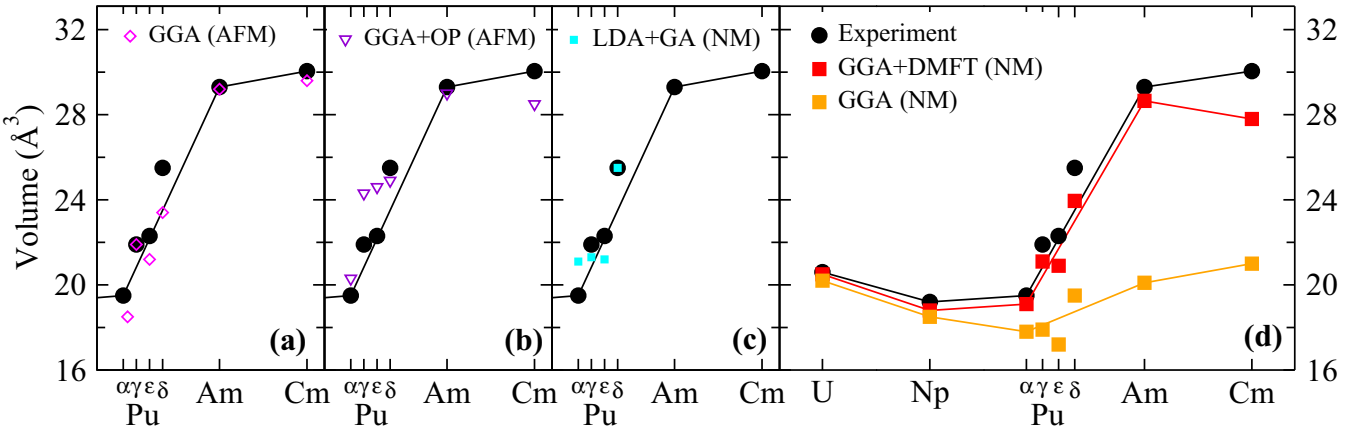

FIG. 3. Theoretical volumes for actinides compared to experiment. (d) Theoretical volumes as obtained in DFT/PBE (NM) and in DFT/PBE+DMFT—with calculated values of the effective direct Coulomb and Hund interactions (see Fig. 2) in comparison to experiment (extrapolated to 0 K for γ-, ϵ-, and δ-Pu [32]), (a) GGA (AFM) [8,11], (b) GGA+OP (AFM) [12,80], and (c) LDA+GA (NM) [32]. Experimental data are taken from Refs. [81–88]. NM refers to a nonmagnetic calculation without any local, or global static magnetic moment. AFM refers to antiferromagnetic calculations. GGA+DMFT, with the *ab initio* determination of U and J is able to describe the equilibrium volumes of all elements and all phases of Pu without any magnetic moment, in agreement with experiment. See Sec. IV A for a detailed discussion.

curium. However, is has been shown recently [92] that both the equilibrium volume and bulk modulus of α-uranium can still be improved using GGA+U and $U = 1.23$ eV. These results were discussed in Refs. [94,95]. However, interestingly, the GGA+U improvement [96] is similar in magnitude to the improvement brought by GGA+DMFT in our work.

2. *Phases of plutonium: structural properties*

We start this section by outlining some experimental data concerning plutonium. Concerning the structural data for the γ, δ, and ϵ phases of plutonium, which are stable only at high temperature, one needs to extrapolate the volume of the phases at zero temperature in order to compare to *ab initio* calculations at 0 K. This has been done my Lanata *et al.* [32] and the corresponding volumes are given in Table II and Fig. 3.[4] Nevertheless, our DFT+DMFT calculations are done at finite electronic temperature but we do not take into account the electronic entropy nor the role of phonons, so that the effect of temperature is only contained in the internal energy. Besides, the internal energy differences are identical for 800 and 200 K, so structural properties are nearly identical for these two temperatures. So we can assume that our ground-state properties would be very similar at zero temperature. This is why we can compare our DFT+DMFT calculations of ground-state properties to 0 K extrapolated data. Concerning the magnetic properties of plutonium, the experimental work of Lashley *et al.* [6] underlines the absence of local moment in plutonium, and thus, according to the authors [6], it rules out the possibility of ordered or disordered local moment in α or δ plutonium.

Our GGA+DMFT structural properties (Table II and Fig. 3) show an overall good agreement with experimental data, of the same quality as the combination of LDA and Gutzwiller approximation [32]. Interestingly, the volume of α phase is even slightly better reproduced by our GGA+DMFT in comparison to LDA+GA [32]. We underline that we do the calculation for the pseudo-α phase [79], but we show in Ref. [46] (Sec. III) that the GGA+DMFT results for the pseudo-α phase and the exact α phase are rather similar. GGA (AFM) [7,8] gives also a similar good description, at the expense, however, of creating an artificial ordered magnetism.

Söderlind and coworkers used the combination of GGA with orbital polarization (OP) [80] to study the phases of actinides. This orbital polarization is "mean-field correction of the intra-atomic Coulomb interaction" [97] of 5f electrons, proportional to the quantum number corresponding to the projection of the angular momentum. These calculations [80] give also a good overall description, except for γ and ϵ phases, where the agreement with 0 K extrapolated data is less good. However, the agreement of GGA+OP calculations at 0 K with experiments at high temperature is better. Another GGA+OP calculation [98] with only an orbital magnetic moment and no spin moment gives also good structural parameters, but, however, magnetic properties are still in disagreement with experiments in which there is not spin or orbital magnetic moment, local or not [6]. In conclusion of this section, we outline that GGA+DMFT (as LDA+GA) is able to describe the phases of plutonium, without the creation of an artificial [6] magnetism.

3. *Phases of plutonium: energetics*

We now discuss the energetic stability of phases of plutonium (see Table II). We find in agreement with experiment and other theoretical methods [GGA (AFM), GGA+OP (AFM), LDA+GA (NM)] that the α phase is the most stable phase of plutonium. The energetic order of other phases is also in agreement with some other theoretical methods. We find that the ϵ phase is slightly lower (-20 meV) in energy in comparison to the δ phases. It does not agree with the Hubbard-I results of Ref. [21] (20 meV). In this last study, indeed, the entropy is viewed as responsible for the stabilization of the ϵ phase. However, we underline that a slight increase of Coulomb interactions ($U = 1$ eV and $J = 0.5$ eV instead of $U = 0.94$ eV and $J = 0.46$ eV) in our calculation can change

[4]This extrapolation has, of course, some degree of arbitrariness.

TABLE II. Structural parameters of uranium, neptunium, americium, curium and some phases of plutonium obtained in this work in comparison to various other methods and experiment. NM, AFM, and OP stand for nonmagnetic calculation, antiferromagnetic calculation, and orbital polarization (see Sec. IV A 2). See also Ref. [46], Sec. I for a benchmark of our NM GGA calculations with other calculations.

	α U	α Np	$\widetilde{\alpha}$-Pu	α-Pu	δ-Pu	γ-Pu	ϵ-Pu	Am	Cm
Experiment [81,83,85,86,88,99]									
V (Å^3)	20.6 [81]	19.2 [100]		20.08 [83]	25.0 [99]	23.5 [99]	24.4 [99]	29.3 [86]	30.05 [88]
B_0(GPa)	115 [81]	120 [101]		54 [83]	29–30 [99]	25.7 [99]	45 [99]	29.7 [86]	30.5 [88]
Experiment extrapolated to 0 K (Lanata *et al.* [32,102])									
V (Å^3)				19.5	25.5	21.9	22.3		
B_0 (GPa)				70 [84]	38				
GGA/SOC+DMFT (NM) (this work)									
V (Å^3)	20.5	18.8	19.1		24.7	21.1	20.9	28.7	27.8
B_0 (GPa)	124	148	110		36	41	34	33.8	36
E (meV)			0		210	100	190		
GGA/SOC (NM) (this work)									
V (Å^3)	20.2	18.5	18.0	17.8	19.5	17.9	17.2	19.9	20.8
B_0 (GPa)	139	174	193	141	86	124	142	61	54
E (meV)			0	–45	700	400	380		
LDA/SOC+GA (NM) [32] 0 K ($U = 4.5$ eV, $J = 0.36$ eV)									
V (Å^3)				21.1	25.5	21.3	21.2		
B_0 (GPa)				50–70	15–35	45–70	35–55		
E (meV)				0	26	9	72		
GGA	NM	NM		AFM	AFM	AFM	AFM	AFM	AFM
V (Å^3)	20.2 [81]	18.4–18.8 [82,103]		18.5 [8]	23.4 [8]	21.9 [8]	21.2 [8]	29.2 [11]	29.34 [11]
B_0 (GPa)	134 [81]	158–170 [82,103]		101 [8]	55 [8]	45 [8]	45 [8]	28.3 [11]	40.3 [11]
E (meV)				0 [8]	122 [8]	109 [8]	175 [8]		
GGA/SOC+OP (AFM) [12,80]									
V (Å^3)				20.3	24.9	24.3	24.6	29	28.5
B_0 (GPa)				50	41	33	23		
E (meV)				0	20	15	110		

the energetic order of these two phases. So, we cannot be conclusive concerning the relative energetic stability of ϵ and δ phases. We will discuss in more details the interplay of correlation and crystal structure in Fig. 5 and Sec. V B 1.

4. Americium and curium

For americium and curium, the GGA+DMFT gives structural properties that are comparable to experiment. Other methods based on magnetic GGA [11,12] give also a good (or even better) agreement with experiment. It is noticeable that GGA+DMFT is able to do it without any local magnetic moment. Indeed, americium carries no local moment. Curium is antiferromagnetic under 65 K and paramagnetic above. We focus our DFT+DMFT calculations on the paramagnetic phase both for simplicity and also because structural parameters [88] and spectral functions [91] are determined in the room-temperature paramagnetic phase. We discuss in the next section the comparison with other DFT+DMFT works [33].

B. Comparison to other calculations for the same effective interactions

Three papers [20,32,33] relate DFT+DMFT or DFT+GA calculations of structural properties of pure actinides. These calculations, however, use three different computational settings (see also Table III): (a) GGA+DMFT calculations [20] with $J = 0$ eV, but with a large (4.0 eV) value of U on plutonium, (b) LDA+GA calculations with large U (4.5 eV) and J (0.36 eV) [32] on plutonium, and (c) LDA+DMFT

TABLE III. Comparison of our DFT+DMFT calculations (*) of volumes and bulk moduli with other DFT+DMFT calculations and DFT+GA calculations. For completeness, we show the structural data obtained with our *ab initio* interactions, and with the interactions proposed by some authors. IS stands for interpolation scheme (see Ref. [20]).

	U, J (eV)	V(Å^3)	B_0(GPa)
δ-plutonium			
GGA+DMFT/CTQMC*	0.94, 0.46	24.0	46
LDA+GA [32]	4.50, 0.36	25.5	15–35
LDA+DMFT/CTQMC*	4.50, 0.36	24.3	43
GGA+DMFT/IS [20]	4.00, 0.00	26.5	
GGA+DMFT/CTQMC*	4.00, 0.00	25.8	28
Americium			
GGA+DMFT/CTQMC*	1.53, 0.42	28.7	33
LDA+DMFT/Hubbard I [33]	4.50, 0.60	27.4	45
LDA+DMFT/CTQMC*	4.50, 0.60	28.0	44

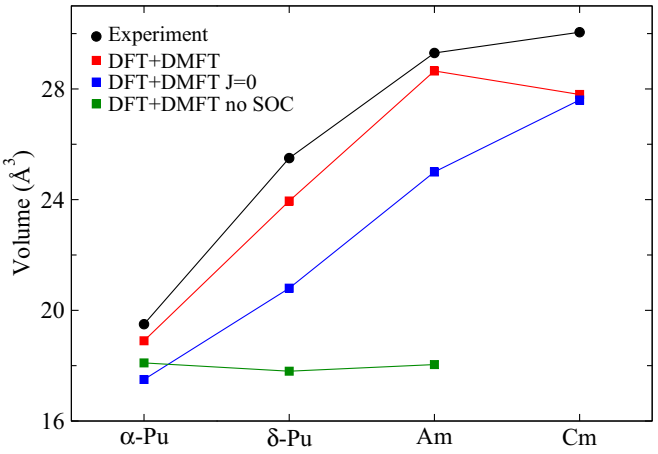

FIG. 4. Role of spin-orbit coupling (SOC) and exchange. Volumes (per atom) of α-Pu, δ-Pu, and Am for the full DMFT calculations (with J and SOC), for calculations without exchange J and for calculations without SOC, in comparison to experiment. The nonmagnetic calculation for curium is not stable without spin-orbit coupling. These calculations show that the combination of both the spin-orbit coupling and exchange J is necessary to recover the equilibrium volume of δ-Pu and Am.

(Hubbard I approximation) calculations with large U (4.5 eV) and J (0.6 eV) on americium [33]. In these published works, indeed, high values of U were used. Moreover, in Ref. [32], the value of J was adapted in order to have a better agreement with experiment. So, there was really a need for an *ab initio* calculation of effective interactions.

Before comparing the calculations to ours, we first check that we recover the results of these papers with the same settings (U, J, DFT functional) but with our computational schemes. Our results are reproduced in Table III. Overall, the agreement is good between our calculation and the cited works [20,32,33], and the differences are in the range of what is expected knowing the various possible definition of correlated orbitals and the differences in the impurity model solver used. This comparison of our calculations and the literature is a further validation of our numerical DFT+DMFT scheme.

Secondly, we find an overall rather good agreement between our GGA+DMFT calculations with an *ab initio* (small U) effective interactions and the above mentioned references [20,32,33].

So indeed, for plutonium and americium, three effects play roughly a similar role concerning the increase of equilibrium volumes: (a) a large value of $U = 4$ eV instead of a small U,[5] (b) the use of $J \simeq 0.5$ eV instead of $J = 0$ eV (see Fig. 4), (c) the use of GGA instead of LDA.[6] Our analysis therefore suggests that high values of U were probably postulated in early works because they were necessary to describe the structural properties of δ plutonium or americium, if exchange interactions were neglected [20] or if the LDA was used instead of the GGA [32,33].[7] Such a variety of DFT+DMFT schemes underlines the need for an *ab initio* determination of the effective interactions as done in this work.

V. DFT+DMFT CALCULATIONS OF STRUCTURAL PROPERTIES OF ACTINIDES: ANALYSIS

We have seen that our calculations are able to reproduce the main trends of structural properties of pure actinides. So in this section, we use our *ab initio* scheme to understand the physical origin of the increase of volume in actinides.

A. Interplay of spin orbit coupling and Hund's coupling

We first highlight the physical effect of the spin-orbit coupling (SOC), and the Hund's exchange J: we suppress successively these two terms in the calculations. Figure 4 shows that the volume of both localized phases (δ-Pu and Am) and delocalized (α-Pu) phases decrease in both cases. Thus the combination of SOC and J is necessary for the description of localized actinides and especially δ-Pu and Am. The importance of Hund's coupling has been underlined recently [38]: indeed, following the so-called Hund's rule, the Hund's exchange restricts the dimension of the Hilbert space and can increase the role of correlation [24,26]. We show here that it has a key role for the determination of structural parameters. Indeed, in plutonium, the Hund's coupling induces that the average interaction [104] between $5/2$ and $7/2$ orbitals ($U_{5/2\text{-}7/2} = 0.78$ eV) is larger than $U_{7/2\text{-}7/2} = 0.67$ eV, which is itself larger than $U_{5/2\text{-}5/2} = 0.62$ eV. Thus, if J increases, the number of electrons inside the $5/2$ shell increases in order to minimize the interactions, and the average local interaction energy inside this shell increases. This is related to the third Hund's rule for atoms; for an atom with less than 7 f electrons, the $5/2$ shell is first filled to reduce the Coulomb interaction. The role of J is thus to fill the $5/2$ shell. As a consequence, the configuration space is reduced in comparison to $J = 0$, and correlations effects are enhanced [38,105]. It thus leads to a larger volume, as expected when correlation effects increase.

B. Role of the crystal structure

As our scheme can describe the experimental volumes, we will use it to disentangle the role of interactions and atomic structure on the jump in volume.

1. Interplay of crystal structure dependent chemical bonding and interaction

First of all, we discuss here and in Fig. 5 two main effects of correlations on the structural properties of localized and delocalized phases, taking α-Pu and δ-Pu as an example: both are the result of the competition of chemical bonding and

[5]Indeed, the use of a large value of U in combination with our calculated value of J leads to an overestimation of volume of δ-Pu; for $U = 3.3$ eV, we find $V = 28.8$ Å^3, much larger than the experimental volume. Using a large value of U in americium, would also lead to an overestimation of volume with respect to experiment.

[6]For δ plutonium, an LDA+DMFT calculation with $U = 3.3$ eV and $J = 0.5$ eV gives a volume of 23.7 Å^3, whereas a GGA+DMFT calculation with the same parameters gives a volume of 28.8 Å^3.

[7]The difference between GGA+DMFT and LDA+DMFT underlines the need for a more advanced scheme, such as GW+DMFT.

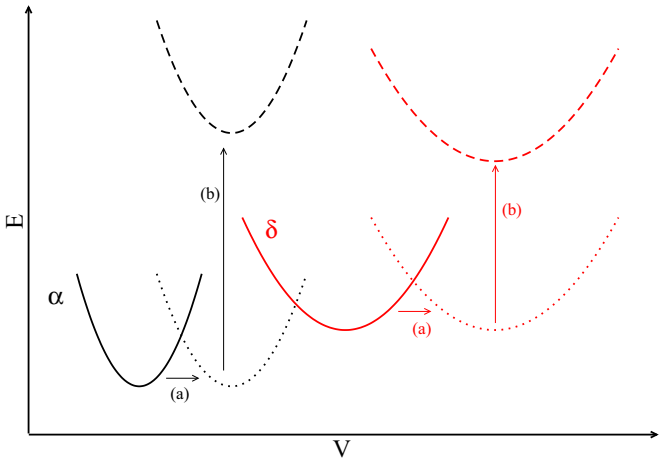

FIG. 5. Sketch of the role of interactions for two different phases. The parabolic curves represent total energy vs volume, and the minima of the curves represent the equilibrium volume. We call α a delocalized phase with an important chemical bonding, and a low symmetry and volume (such as α-U, α-Np, or α-Pu), whereas δ is a compact phase (such as fcc Pu, or dhcp Am), with large interatomic distances. (a) and (b) are two effects induced by electronic interactions (see discussion in Sec. V B 1). As discussed in the text (see Secs. V B 1 and V D), we emphasize that even with the same U and J, α-Pu, and δ-Pu have very different equilibrium volumes in DFT+DMFT because of their different chemical bonding.

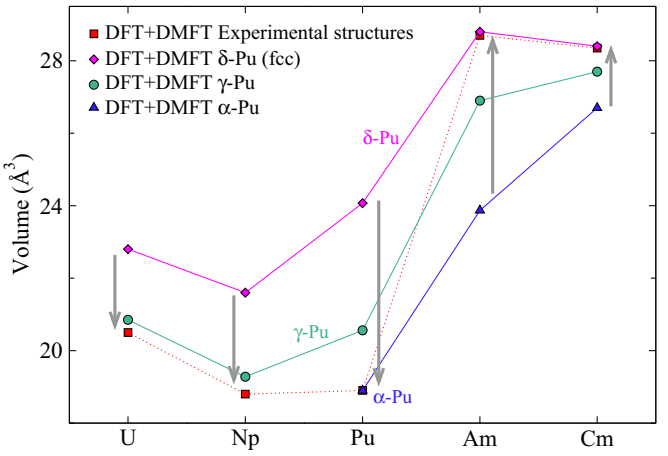

FIG. 6. Role of crystal structure on theoretical volumes. Comparison of DFT+DMFT calculations of volumes (per atom) for actinides with the fcc structure, γ-Pu structure, δ-Pu structure, and experimental structures. Arrows show the direction of the decrease of DFT+DMFT energy towards the most stable phase (in agreement with experiment). For example, for plutonium, we indeed found that the α phase is more stable than the γ phase, whereas the δ fcc phase is less stable, in agreement with experiment.

strong interactions. (a) The first effect concerns the equilibrium volumes: local interactions are known to increase the volume of solids. However, as chemical bonding is stronger in α Pu with respect to the fcc δ-phase, correlation has a larger effect on the structural properties of the fcc phase, leading to a outstanding increase of the volume for the compact (fcc) δ phase with respect to the α phase because of correlation (see DFT versus DFT+DMFT data on Fig. 3). (b) The second effect concerns the stability of phases: as chemical bonding and thus delocalization of electrons are larger for the α phase, the electronic interaction is larger—because it is compensated by the bonding—and thus the α phase is destabilized (by interactions) with respect to the fcc δ phase, for which bonding and thus electronic interactions are weaker. The consequence of this destabilization depends on the element: for early actinides (U, Np), there are only a few $5f$ electrons, thus the interaction energy is weak and delocalized distorted structures (α-U and α-Np) are still stable with respect to the fcc phase. For late actinides, interactions are so important that compact phases (fcc/dhcp) are more stable than delocalized phases. For example, we compare interactions effects in uranium and plutonium which have roughly the same U and J (see Fig. 2), and the α phases of the two elements have low volumes: as plutonium has more $5f$ electrons than uranium, the impact of interactions on the stability of phases is larger and lead to the energetic proximity of the α and fcc phases of plutonium. Indeed, for plutonium, DMFT decreases the energy difference between the fcc phase and α phase from 700 meV (GGA) to 210 meV (GGA+DMFT). For uranium, the role of DMFT on the same energy difference is weak (some meV). For americium, the role of DMFT is huge and invert the stability of phases.

2. *Impact of the crystal structure on the jump in volume*

As we just saw, the correlation have different effects on different phases, so that atomic structure and correlation effects are intricate. So, we compare now the evolution of volume as a function of Z for fixed structures: we choose the fcc, γ-plutonium, and α-plutonium structures. Notice that the coordination and the first nearest-neighbor bond lengths—for the same volume—are decreasing from fcc to γ-Pu and α-Pu (see Ref. [46], Sec. III). DFT+DMFT results are given in Fig. 6, and we now discuss the evolution of volumes for the three structures, thanks to the general features described above and in Fig. 5. First, the fcc structure, because of its compactness, has a large first-neighbors distance, that favors localized electron phases. This has two consequences: firstly, for lighter actinides, the fcc volumes are higher, and thus the volume jump is smaller. Secondly, the jump happens early (for plutonium, instead of americium). Indeed, the fcc structure is more sensitive to interactions. On the contrary, if we constrain the system to adopt the α-plutonium structure and only relax the volume, the jump is weaker and appears for americium, because this phase is less sensitive to interaction effects. For the γ-plutonium phase, we find an intermediate behavior and still an important jump for americium. So our calculations highlight that the experimental jump of the volume is due to electronic effects, because one recovers the jump for a fixed common structure [(a) effect], but the jump is exacerbated by the correlation-induced stabilization effects of localized or delocalized phases [(b) effect].

C. Role of effective interaction and number of electrons

We now discuss the electronic origin of the jump. So we do not discuss here the relative stability of the phases (which was discussed in the previous section), but the shift of volume due to DMFT for a fixed structure, as a function of Z. Two main

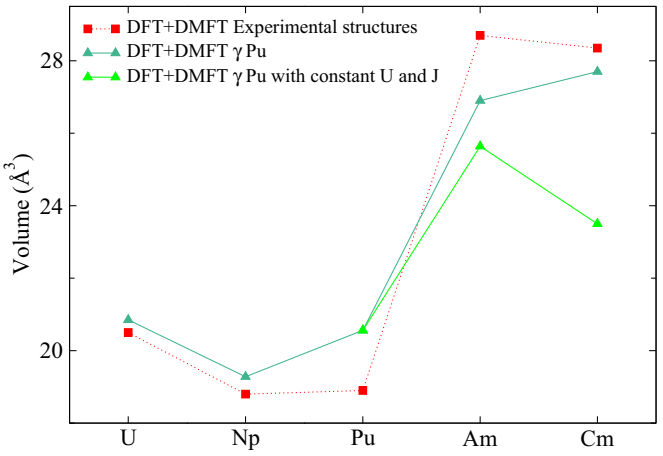

FIG. 7. DFT+DMFT calculations of volumes (per atom) for actinides, with the same imposed structure (the γ phase of plutonium). The graph compares calculations with computed U and J for each actinides, with calculations with a fixed U and J. For reference, DFT+DMFT calculations for experimental structures are also given.

tendencies play a role. First, when Z increases, the localization of orbitals increases and moreover the effective interactions are more important, as can be seen in Fig. 2: both the bare and effective interactions increase when Z increases. The second effect is the increase of the number of electrons when Z increases. In order to disentangled these two effects, we carried out a calculation for fixed $U = 0.94$ eV and $J = 0.46$ eV values for Pu, Am, and Cm with the same γ-Pu structure. Then, in Fig. 7, we compare these calculations with calculations done with the cRPA computed U and J for each actinides. The results are contrasted: the jump in volume from plutonium to americium is kept with a constant U and J. So this jump is mainly due to the increase of the band filling. However, with these values of U and J, the volume of curium is small. Indeed, for curium, the effect of J is weak (see Fig. 4) and a high value of U, as determined by our scheme, is necessary for a good description of the structural properties. So our overall conclusion is that the electronic origin of the jump is a complex combination of the spin-orbit coupling effect, band filling, and increase of localization.

D. Which elements and phases are strongly correlated?

In this section, we discuss which actinides or phases are strongly correlated and which are weakly. A pragmatic view is to see strongly correlated systems as those where DFT/LDA-GGA fails. If one thus takes as reference GGA (AFM) calculations, the main improvement induced by DFT+DMFT is the correct description of magnetism. As the existence of magnetism itself is caused by electronic interactions, this failure of GGA (AFM) to recover the correct magnetism for Pu, Am, and Cm can be seen as a proof that electronic interactions are important in these systems. If one takes as a reference GGA (NM) calculations, then the DFT+DMFT main improvement is in the description of structural properties and again the main effect is on Pu, Am and Cm.

Now, we discuss the effect of correlations on the phases of Pu. In order to evaluate the effect of correlations (induced by DMFT) on pressure of these phases, an important quantity is the difference in pressure [32] between GGA and GGA+DMFT (NM) $P_{\mathrm{GGA}}(V) - P_{\mathrm{GGA+DMFT}}(V) = d(E_{\mathrm{GGA+DMFT}}(V) - E_{\mathrm{GGA}})(V)/dV$. We find that this shift is (nearly) the same for α and δ phases.[8]

However, in practice, the impact of Coulomb interactions on both phases is very different: DFT+DMFT increases dramatically the lattice parameter of δ phase, whereas the lattice parameter of the α phase is only slightly increased (see, e.g., Fig. 3). So how can we reconciliate the large impact on volume but the weak impact on difference of pressure? The origin of this difference of behavior—already emphasized by Lanata *et al.* [32]—is that the α phase has stronger chemical bonds (hence a larger bulk modulus), and thus, as discussed in Sec. V B 1 and on Fig. 5, is less sensitive to interactions in comparison to the δ phase. Indeed the shift in volume depends on the variation of the pressure as a function of volume, which is in particular related to the bulk modulus B_0. So interactions are important for total energy and pressure in both the α and δ phases as discussed earlier [20] but the impact of interactions on lattice parameters is weaker in α. It is thus the balance between chemical bonding and interaction which is important to evaluate if interactions will have an impact on structural properties.

VI. CONCLUSION

In conclusion, we underlined the stringent need for a calculation of interactions to describe structural properties in pure actinides. Our calculations highlight that the physical origin of the jump in actinides is twofold. First, as commonly though, the jump has an electronic origin. Second, this jump is exacerbated by correlation induced stabilization of localized phases (for Am and Cm), or delocalized phases (for U, Np, and Pu). This work opens the way to future work concerning first-order structural phase transitions under pressure or temperature in actinides, lanthanides, and alloys.

ACKNOWLEDGMENTS

We thank F. Bottin, J. Bouchet, C. Denoual, B. Dorado, F. Jollet, and G. Robert for useful discussions about this work. We thank Jennifer Milne for proofreading some part of the paper.

APPENDIX A: CALCULATION OF EFFECTIVE INTERACTIONS PARAMETERS: EVALUATION OF PRECISION

1. Comparison of DFT+U and DFT+DMFT spectral functions

Our scheme to compute U is parameter-free. However, it relies on a DFT+U description of pure actinides. As we have shown, DFT+DMFT offers a good description of pure actinides and thus a self-consistent calculation of U within DFT+DMFT or GW+DMFT would be indeed more accurate.

[8]Note that this is not in contradiction to the fact that the internal energy increase is larger in the α phase as discussed in Sec. V B 1. Indeed, $E_{\mathrm{GGA+DMFT}}(V) - E_{\mathrm{GGA}}(V)$ is much larger in the α phase with respect to the δ phase, but this difference is independent of volume and disappears in the derivative.

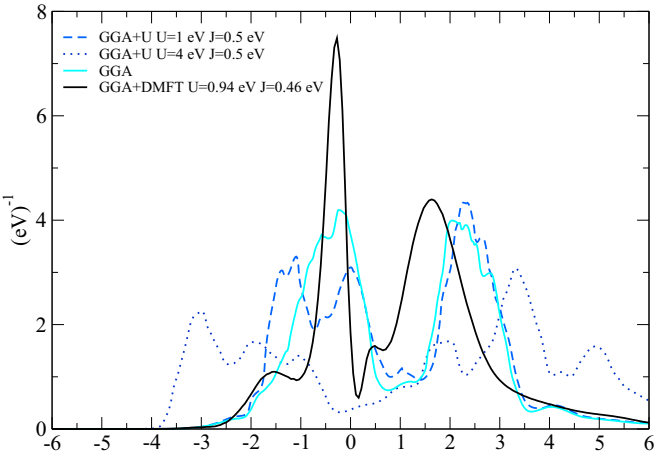

FIG. 8. DFT+DMFT 5f spectral functions of δ-Pu compared to the GGA and GGA+U 5f projected density of states (DOS) used for the cRPA calculation of U. Calculations are done at 800 K and GGA+U and GGA DOS are widened (with a 0.5 eV broadening) to be easily compared to DFT+DMFT spectral function.

However, as discussed before, a full implementation of these framework is still in progress and its application to actinides would be even more demanding than the current work.

However, as DFT+U can be viewed as the (broken-symmetry) limit of DFT+DMFT in the case where correlation is strong, we can expect the screening to be more efficient in DFT+DMFT because electrons will be less localized. So, the value of effective interactions that we obtain in DFT+U should be an overestimation of the more complete dynamical effective interactions computed in GW+DMFT. A rough way to see if the screening is similar is to compare the spectral functions computed by the two methods. Figure 8 displays first the DFT+DMFT spectral function. We also plot the DFT+U spectral functions (GGA+U ferromagnetic without SOC) computed for $U = 1$ eV and also $U = 4$ eV in comparison to DFT+DMFT and GGA calculations. The DFT+DMFT spectral functions are indeed much closer to the DFT+U with $U = 1$ eV and the GGA.[9] The position of the correlated bands is important because the important transitions for the screening are the transitions inside the noncorrelated bands (not plotted) and more importantly from the correlated f bands to noncorrelated bands [37]. So, this comparison shows the following: the position of the f peaks is closer to the Fermi level in DFT+DMFT in comparison to GGA and DFT+U. Thus, neglecting dynamical effects, the value of U computed in DFT+DMFT should be slightly lower than the cRPA obtained from GGA or DFT+U.

Nevertheless, we will see that the main effect concerning structural properties—at least for Pu and Am—is the value of the Hund's coupling J, which is known to be much less sensitive to screening, as can be seen in Table I. So we can be confident that our physical findings are robust and are independent of a small variation of U.

[9]Indeed, it was seen also in Ref. [26] that the GGA density of states has a structure similar to the DMFT spectral function.

2. Variation of the cRPA computed U for different band structure

Here, we evaluate the role of the band structure on the value of U as computed in cRPA. Indeed, even the value of U is weakly dependent on the band structure: we carried out calculations of U within cRPA with DFT+U band structure with increasing values of U. In these calculations, thus, the DFT+U spectral function shows important variations as U increases. We found that the cRPA computed U varies from 0.9 eV (with the GGA band structure) to only 2.2 eV (for the GGA+U band structure with $U = 4$ eV). These values reinforce our conclusion that in plutonium, the value of the direct Coulomb interaction is weak.

Concerning americium, even using a DFT+U band structure with $U = 4.5$ eV and $J = 0.5$ eV, gives a value for U of 2.3 eV, still a weak value. It thus confirms that the direct Coulomb interaction is weak.

APPENDIX B: DFT+DMFT: ELECTRONIC PROPERTIES AND SPECTRAL FUNCTIONS

Describing the electronic properties is not the goal of our scheme. Indeed, as we use an efficient density-density approximation for the CTQMC solver, we do not expect a high precision on spectra as we cannot recover the multiplet structure. However, as we will see below, the most important electronic properties of actinides are recovered.

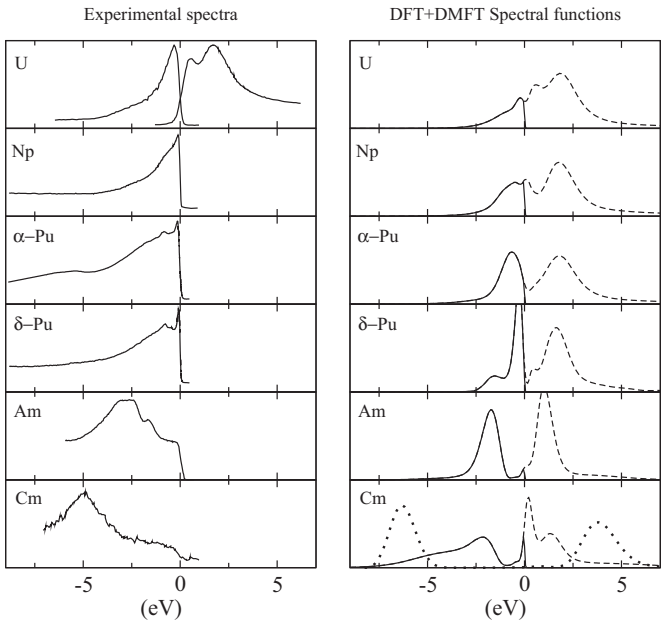

FIG. 9. Experimental photoemission spectra (left) of α-uranium (398 K) [106], α-neptunium (80 K) [107], plutonium (α at 423 K and δ at 77 K) [108], americium (at 298 K) [109], and curium (298 K) [91], compared to our DFT+DMFT spectral functions (right) computed with *ab initio* effective interactions computed with the self-consistent cRPA scheme. The full spectral function, and theoretical direct photoemission spectra are presented in dashed and full lines, respectively. Results are nearly identical at 800 and 200 K. Magnetic calculations for curium are indicated by dotted lines.

1. Number of electrons

For plutonium, we find a number of $5f$ electrons of 5.05 in agreement with the published results [22,24–26], which give values between 5.0 and 5.2. The number of electrons can indeed change slightly as a function of the definition of the correlated orbitals or Wannier functions. Concerning americium, we recover the main results of Ref. [33]: the $5/2$ shell is filled with 5.75 electrons and only 0.29 electrons are in the $7/2$ shell. We performed DFT+DMFT calculations for ferromagnetic curium, and in this case, the second Hund's rule becomes more important than the third, as noticed before [24]. Moreover, we find that, because of the GGA exchange mainly, the number of electrons in the $5/2$ and $7/2$ shells are respectively 3.77 and 2.84, in agreement with the results of Ref. [24] also for the magnetic case.

The calculations in this paper are focusing on DFT+DMFT calculations on paramagnetic curium, which is the stable phase above 65 K [91]. In this case, we found on average a filled $5/2$ shell and one electron in the $7/2$ shell. Moreover, we found logically a weak effect of J (see Fig. 3 of the letter) because the $5/2$ shell is completely filled, and the main physical effect on structural properties originates here from the direct Coulomb interaction U, which is large in this case (see Table I). These nonmagnetic calculations thus differ from the results of Ref. [110], which find 4.04 and 3.03 electrons, respectively, for the $5/2$ and $7/2$ shells. As discussed below, the difference could arise from our simplified density-density CTQMC solver.

2. Spectral functions

In Fig. 9, we plot the experimental photoemission spectra of uranium, neptunium, plutonium, americium, and curium, and the inverse photoemission spectrum of uranium in comparison to our DFT+DMFT calculations.

Our calculations reproduce the main trends of the experimental data; for early actinides (uranium, neptunium), the calculations reproduce the structures around the Fermi level. For plutonium, the appearance of peaks at the Fermi level is roughly taken into account. Besides, the spectral function of plutonium for the δ phase is in reasonable agreement with Ref. [26] in particular concerning the position of the peaks even if we use completely different values of interactions. For late actinides, the appearance of high energy structures is reproduced, even if the position of the peaks is not perfect.

We emphasize that americium and curium are localized systems, where the description of multiplets might be important. We cannot expect to describe the photoemission spectra in these systems. Indeed, this work uses an efficient density-density CTQMC solver to focus mainly on the structural properties. Analyzing spectral functions would probably require a much more computationally expensive rotationally invariant solver, and is not the goal of this work.

[1] K. T. Moore and G. van der Laan, Nature of the 5f states in actinide metals, Rev. Mod. Phys. **81**, 235 (2009).

[2] P. Söderlind, First-principles phase stability, bonding, and electronic structure of actinide metals, J. Electron Spectrosc. Relat. Phenom. **194**, 2 (2014).

[3] C. Bonnelle and N. Spector, Electron distributions and crystalline structures, in *Rare-earths and Actinides in High Energy Spectroscopy* (Springer, Dordrecht, Netherlands, 2015), pp. 1–78.

[4] A. McMahan, C. Huscroft, R. Scalettar, and E. Pollock, Volume-collapse transitions in the rare earth metals, J. Comput.-Aided Mater. Des. **5**, 131 (1998).

[5] I. L. M. Locht, Y. O. Kvashnin, D. C. M. Rodrigues, M. Pereiro, A. Bergman, L. Bergqvist, A. I. Lichtenstein, M. I. Katsnelson, A. Delin, A. B. Klautau, B. Johansson, I. Di Marco, and O. Eriksson, The standard model of the rare-earths, analyzed from the Hubbard I approximation, Phys. Rev. B **94**, 085137 (2016).

[6] J. C. Lashley, A. Lawson, R. J. McQueeney, and G. H. Lander, Absence of magnetic moments in plutonium, Phys. Rev. B **72**, 054416 (2005).

[7] Y. Wang and Y. Sun, First-principles thermodynamic calculations for δ-Pu and ε-Pu, J. Phys.: Condens. Matter **12**, L311 (2000).

[8] G. Robert, A. Pasturel, and B. Siberchicot, Calculated thermodynamic properties of plutonium metal, J. Phys.: Condens. Matter **15**, 8377 (2003).

[9] P. Söderlind, F. Zhou, A. Landa, and J. E. Klepeis, Phonon and magnetic structure in δ-plutonium from density-functional theory, Sci. Rep. **5**, 15958 (2015).

[10] P. Söderlind, K. T. Moore, A. Landa, B. Sadigh, and J. A. Bradley, Pressure-induced changes in the electronic structure of americium metal, Phys. Rev. B **84**, 075138 (2011).

[11] A. Kutepov and S. Kutepova, First-principles study of electronic and magnetic structure of α-Pu, δ-Pu, americium, and curium, J. Magn. Magn. Mater. **272–276**, E329 (2004).

[12] P. Söderlind, G. Kotliar, K. Haule, P. M. Oppeneer, and D. Guillaumont, Computational modeling of actinide materials and complexes, MRS Bull. **35**, 883 (2010).

[13] A. Svane, L. Petit, Z. Szotek, and W. M. Temmerman, Self-interaction-corrected local spin density theory of $5f$ electron localization in actinides, Phys. Rev. B **76**, 115116 (2007).

[14] J. Bouchet, B. Siberchicot, F. Jollet, and A. Pasturel, Equilibrium properties of δ-Pu: LDA+U calculations, J. Phys.: Condens. Matter **12**, 1723 (2000).

[15] S. Y. Savrasov and G. Kotliar, Ground State Theory of δ-Pu, Phys. Rev. Lett. **84**, 3670 (2000).

[16] A. K. Verma, P. Modak, S. M. Sharma, A. Svane, N. E. Christensen, and S. K. Sikka, Theoretical investigation of pressure-induced structural transitions in americium using GGA + U and hybrid density functional theory methods, Phys. Rev. B **88**, 014111 (2013).

[17] A. B. Shick, A. I. Liechtenstein, and W. E. Pickett, Implementation of the LDA+U method using the full-potential linearized augmented plane-wave basis, Phys. Rev. B **60**, 10763 (1999).

[18] B. Amadon, F. Jollet, and M. Torrent, γ and β cerium: LDA+U calculations of ground-state parameters, Phys. Rev. B **77**, 155104 (2008).

[19] G. Kotliar, S. Y. Savrasov, K. Haule, V. S. Oudovenko, O. Parcollet, and C. A. Marianetti, Electronic structure calculations with dynamical mean-field theory, Rev. Mod. Phys. **78**, 865 (2006).

[20] S. Y. Savrasov, G. Kotliar, and E. Abrahams, Correlated electrons in delta-plutonium within a dynamical mean-field picture, Nature (London) **410**, 793 (2001).

[21] X. Dai, S. Y. Savrasov, G. Kotliar, A. Migliori, H. Ledbetter, and E. Abrahams, Calculated phonon spectra of plutonium at high temperatures, Science **300**, 953 (2003).

[22] L. V. Pourovskii, G. Kotliar, M. I. Katsnelson, and A. I. Lichtenstein, Dynamical mean-field theory investigation of specific heat and electronic structure of α and δ-plutonium, Phys. Rev. B **75**, 235107 (2007).

[23] A. Shick, J. Kolorenc, L. Havela, V. Drchal, and T. Gouder, Multiplet effects in the electronic structure of δ-Pu, Am and their compounds, Europhys. Lett. **77**, 17003 (2007).

[24] J. H. Shim, K. Haule, and G. Kotliar, Fluctuating valence in a correlated solid and the anomalous properties of δ-plutonium, Nature (London) **446**, 513 (2007).

[25] J.-X. Zhu, A. K. McMahan, M. D. Jones, T. Durakiewicz, J. J. Joyce, J. M. Wills, and R. C. Albers, Spectral properties of δ-plutonium: Sensitivity to 5f occupancy, Phys. Rev. B **76**, 245118 (2007).

[26] C. A. Marianetti, K. Haule, G. Kotliar, and M. J. Fluss, Electronic Coherence in δ-Pu: A Dynamical Mean-Field Theory Study, Phys. Rev. Lett. **101**, 056403 (2008).

[27] E. Gorelov, J. Kolorenc, T. Wehling, H. Hafermann, A. B. Shick, A. N. Rubtsov, A. Landa, A. K. McMahan, V. I. Anisimov, M. I. Katsnelson, and A. I. Lichtenstein, Importance of full coulomb interactions for understanding the electronic structure of δ-Pu, Phys. Rev. B **82**, 085117 (2010).

[28] A. Kutepov, K. Haule, S. Y. Savrasov, and G. Kotliar, Electronic structure of Pu and Am metals by self-consistent relativistic GW method, Phys. Rev. B **85**, 155129 (2012).

[29] A. B. Shick, J. Kolorenc, J. Rusz, P. M. Oppeneer, A. I. Lichtenstein, M. I. Katsnelson, and R. Caciuffo, Unified character of correlation effects in unconventional Pu-based superconductors and δ-Pu, Phys. Rev. B **87**, 020505 (2013).

[30] J.-X. Zhu, R. C. Albers, K. Haule, G. Kotliar, and J. M. Wills, Site-selective electronic correlation in α-plutonium metal, Nat. Commun. **4**, 2644 (2013).

[31] M. Janoschek, P. Das, B. Chakrabarti, D. L. Abernathy, M. D. Lumsden, J. M. Lawrence, J. D. Thompson, G. H. Lander, J. N. Mitchell, S. Richmond, M. Ramos, F. Trouw, J.-X. Zhu, K. Haule, G. Kotliar, and E. D. Bauer, The valence-fluctuating ground state of plutonium, Sci. Adv. **1**, e1500188 (2015).

[32] N. Lanatà, Y. Yao, C.-Z. Wang, K.-M. Ho, and G. Kotliar, Phase Diagram and Electronic Structure of Praseodymium and Plutonium, Phys. Rev. X **5**, 011008 (2015).

[33] S. Y. Savrasov, K. Haule, and G. Kotliar, Many-Body Electronic Structure of Americium Metal, Phys. Rev. Lett. **96**, 036404 (2006).

[34] F. Aryasetiawan, M. Imada, A. Georges, G. Kotliar, S. Biermann, and A. I. Lichtenstein, Frequency-dependent local interactions and low-energy effective models from electronic structure calculations, Phys. Rev. B **70**, 195104 (2004).

[35] K. Karlsson, F. Aryasetiawan, and O. Jepsen, Method for calculating the electronic structure of correlated materials from a truly first-principles LDA+U scheme, Phys. Rev. B **81**, 245113 (2010).

[36] B.-C. Shih, Y. Zhang, W. Zhang, and P. Zhang, Screened coulomb interaction of localized electrons in solids from first principles, Phys. Rev. B **85**, 045132 (2012).

[37] B. Amadon, T. Applencourt, and F. Bruneval, Screened coulomb interaction calculations: cRPA implementation and applications to dynamical screening and self-consistency in uranium dioxide and cerium, Phys. Rev. B **89**, 125110 (2014).

[38] A. Georges, L. d. Medici, and J. Mravlje, Strong correlations from Hund's coupling, Ann. Rev. Condens. Matter Phys. **4**, 137 (2013).

[39] B. Amadon, A self-consistent DFT+DMFT scheme in the projector augmented wave method: applications to cerium, Ce_2O_3 and Pu_2O_3 with the Hubbard I solver and comparison to DFT+U, J. Phys.: Condens. Matter **24**, 075604 (2012).

[40] B. Amadon, F. Lechermann, A. Georges, F. Jollet, T. O. Wehling, and A. I. Lichtenstein, Plane-wave based electronic structure calculations for correlated materials using dynamical mean-field theory and projected local orbitals, Phys. Rev. B **77**, 205112 (2008).

[41] J. Bieder and B. Amadon, Thermodynamics of the α-γ transition in cerium from first principles, Phys. Rev. B **89**, 195132 (2014).

[42] B. Amadon, S. Biermann, A. Georges, and F. Aryasetiawan, The α-γ Transition of Cerium Is Entropy Driven, Phys. Rev. Lett. **96**, 066402 (2006).

[43] P. E. Blöchl, Projector augmented-wave method, Phys. Rev. B **50**, 17953 (1994).

[44] M. Torrent, F. Jollet, F. Bottin, G. Zérah, and X. Gonze, Implementation of the projector augmented-wave method in the ABINIT code: Application to the study of iron under pressure, Comput. Mater. Sci. **42**, 337 (2008).

[45] X. Gonze, F. Jollet, F. A. Araujo, D. Adams, B. Amadon, T. Applencourt, C. Audouze, J.-M. Beuken, J. Bieder, A. Bokhanchuk, E. Bousquet, F. Bruneval, D. Caliste, M. Côté, F. Dahm, F. D. Pieve, M. Delaveau, M. D. Gennaro, B. Dorado, C. Espejo, G. Geneste, L. Genovese, A. Gerossier, M. Giantomassi, Y. Gillet, D. Hamann, L. He, G. Jomard, J. L. Janssen, S. L. Roux, A. Levitt, A. Lherbier, F. Liu, I. Lukačević, A. Martin, C. Martins, M. Oliveira, S. Poncé, Y. Pouillon, T. Rangel, G.-M. Rignanese, A. Romero, B. Rousseau, O. Rubel, A. Shukri, M. Stankovski, M. Torrent, M. V. Setten, B. V. Troeye, M. Verstraete, D. Waroquiers, J. Wiktor, B. Xu, A. Zhou, and J. Zwanziger, Recent developments in the `ABINIT` software package, Comput. Phys. Commun. **205**, 106 (2016).

[46] See Supplemental Material at http://link.aps.org/supplemental/10.1103/PhysRevB.94.115148 for the PAW atomic data, the density-density approximation for CTQMC, and the crystallographic structure of plutonium phases.

[47] B. Amadon and A. Gerossier, Comparative analysis of models for the α-γ phase transition in cerium: A DFT+DMFT study using wannier orbitals, Phys. Rev. B **91**, 161103 (2015).

[48] P. Sun and G. Kotliar, Extended dynamical mean-field theory and GW method, Phys. Rev. B **66**, 085120 (2002).

[49] S. Biermann, F. Aryasetiawan, and A. Georges, First-Principles Approach to the Electronic Structure of Strongly Correlated Systems: Combining the GW Approximation and Dynamical Mean-Field Theory, Phys. Rev. Lett. **90**, 086402 (2003).

[50] T. Ayral, S. Biermann, and P. Werner, Screening and nonlocal correlations in the extended hubbard model from self-consistent combined GW and dynamical mean-field theory, Phys. Rev. B **87**, 125149 (2013).

[51] C. Taranto, M. Kaltak, N. Parragh, G. Sangiovanni, G. Kresse, A. Toschi, and K. Held, Comparing quasiparticle GW+DMFT and LDA+DMFT for the test bed material $SrVO_3$, Phys. Rev. B **88**, 165119 (2013).

[52] J. M. Tomczak, M. Casula, T. Miyake, and S. Biermann, Asymmetry in band widening and quasiparticle lifetimes in $SrVO_3$: Competition between screened exchange and local correlations from combined gw and dynamical mean-field theory GW+DMFT, Phys. Rev. B **90**, 165138 (2014).

[53] J. M. Tomczak, QS GW +DMFT: an electronic structure scheme for the iron pnictides and beyond, J. Phys.: Conf. Ser. **592**, 012055 (2015).

[54] S. Biermann, Dynamical screening effects in correlated electron materials. a progress report on combined many-body perturbation and dynamical mean-field theory: GW + DMFT, J. Phys.: Condens. Matter **26**, 173202 (2014).

[55] L. Boehnke, F. Nilsson, F. Aryasetiawan, and P. Werner, When strong correlations become weak: Consistent merging of GW and DMFT, arXiv:1604.02023 [cond-mat.str-el].

[56] P. Werner and M. Casula, Dynamical screening in correlated electron systems - from lattice models to realistic materials, J. Phys.: Condens. Matter **28**, 383001 (2016).

[57] I. Di Marco, J. Minár, S. Chadov, M. I. Katsnelson, H. Ebert, and A. I. Lichtenstein, Correlation effects in the total energy, the bulk modulus, and the lattice constant of a transition metal: Combined local-density approximation and dynamical mean-field theory applied to Ni and Mn, Phys. Rev. B **79**, 115111 (2009).

[58] O. Granas, I. D. Marco, P. Thunstrom, L. Nordstrom, O. Eriksson, T. Bjorkman, and J. Wills, Charge self-consistent dynamical mean-field theory based on the full-potential linear muffin-tin orbital method: Methodology and applications, Comput. Mater. Sci. **55**, 295 (2012).

[59] M. S. Litsarev, I. Di Marco, P. Thunström, and O. Eriksson, Correlated electronic structure and chemical bonding of cerium pnictides and γ-Ce, Phys. Rev. B **86**, 115116 (2012).

[60] K. Held, A. K. McMahan, and R. T. Scalettar, Cerium Volume Collapse: Results from the Merger of Dynamical Mean-Field Theory and Local Density Approximation, Phys. Rev. Lett. **87**, 276404 (2001).

[61] A. K. McMahan, K. Held, and R. T. Scalettar, Thermodynamic and spectral properties of compressed Ce calculated using a combined local-density approximation and dynamical mean-field theory, Phys. Rev. B **67**, 075108 (2003).

[62] I. Leonov, N. Binggeli, D. Korotin, V. I. Anisimov, N. Stojić, and D. Vollhardt, Structural Relaxation Due to Electronic Correlations in the Paramagnetic Insulator $KCuF_3$, Phys. Rev. Lett. **101**, 096405 (2008).

[63] I. Leonov, D. Korotin, N. Binggeli, V. I. Anisimov, and D. Vollhardt, Computation of correlation-induced atomic displacements and structural transformations in paramagnetic $KCuF_3$ and $LaMnO_3$, Phys. Rev. B **81**, 075109 (2010).

[64] I. Leonov, A. I. Poteryaev, V. I. Anisimov, and D. Vollhardt, Electronic Correlations at the α-γ Structural Phase Transition in Paramagnetic Iron, Phys. Rev. Lett. **106**, 106405 (2011).

[65] A. O. Shorikov, S. V. Streltsov, M. A. Korotin, and V. I. Anisimov, Phase stability of α-, γ-, and ε-ce: DFT+DMFT study, JETP Lett. **102**, 616 (2015).

[66] P. Werner, A. Comanac, L. de Medici, M. Troyer, and A. J. Millis, Continuous-time Solver for Quantum Impurity Models, Phys. Rev. Lett. **97**, 076405 (2006).

[67] E. Gull, A. J. Millis, A. I. Lichtenstein, A. N. Rubtsov, M. Troyer, and P. Werner, Continuous-time monte carlo methods for quantum impurity models, Rev. Mod. Phys. **83**, 349 (2011).

[68] M. Aichhorn, L. Pourovskii, and A. Georges, Importance of electronic correlations for structural and magnetic properties of the iron pnictide superconductor LaFeAsO, Phys. Rev. B **84**, 054529 (2011).

[69] G. Lee, H. S. Ji, Y. Kim, C. Kim, K. Haule, G. Kotliar, B. Lee, S. Khim, K. H. Kim, K. S. Kim, K.-S. Kim, and J. H. Shim, Orbital Selective Fermi Surface Shifts and Mechanism of High T_c Superconductivity in Correlated aFeAs (a = Li, Na), Phys. Rev. Lett. **109**, 177001 (2012).

[70] D. Grieger, C. Piefke, O. E. Peil, and F. Lechermann, Approaching finite-temperature phase diagrams of strongly correlated materials: A case study for V_2O_3, Phys. Rev. B **86**, 155121 (2012).

[71] L. V. Pourovskii, T. Miyake, S. I. Simak, A. V. Ruban, L. Dubrovinsky, and I. A. Abrikosov, Electronic properties and magnetism of iron at the earth's inner core conditions, Phys. Rev. B **87**, 115130 (2013).

[72] H. Park, A. J. Millis, and C. A. Marianetti, Total energy calculations using DFT+DMFT: Computing the pressure phase diagram of the rare earth nickelates, Phys. Rev. B **89**, 245133 (2014).

[73] H. Park, A. J. Millis, and C. A. Marianetti, Computing total energies in complex materials using charge self-consistent DFT + DMFT, Phys. Rev. B **90**, 235103 (2014).

[74] J. Chen, A. J. Millis, and C. A. Marianetti, Density functional plus dynamical mean-field theory of the spin-crossover molecule $Fe(phen)_2NCS_2$, Phys. Rev. B **91**, 241111 (2015).

[75] I. Leonov, Metal-insulator transition and local-moment collapse in FeO under pressure, Phys. Rev. B **92**, 085142 (2015).

[76] K. Haule and T. Birol, Free Energy from Stationary Implementation of the DFT + DMFT Functional, Phys. Rev. Lett. **115**, 256402 (2015).

[77] J. P. Perdew, K. Burke, and M. Ernzerhof, Generalized Gradient Approximation Made Simple, Phys. Rev. Lett. **77**, 3865 (1996).

[78] P. Söderlind, O. Eriksson, B. Johansson, and J. M. Wills, Electronic properties of f -electron metals using the generalized gradient approximation, Phys. Rev. B **50**, 7291 (1994).

[79] J. Bouchet, R. C. Albers, M. D. Jones, and G. Jomard, New Pseudophase Structure for α-Pu, Phys. Rev. Lett. **92**, 095503 (2004).

[80] P. Söderlind and B. Sadigh, Density-Functional Calculations of α, β, γ, δ, δ', and ϵ Plutonium, Phys. Rev. Lett. **92**, 185702 (2004).

[81] A. Dewaele, J. Bouchet, F. Occelli, M. Hanfland, and G. Garbarino, Refinement of the equation of state of α-uranium, Phys. Rev. B **88**, 134202 (2013).

[82] P. Söderlind, B. Johansson, and O. Eriksson, Theoretical zero-temperature phase diagram for neptunium metal, Phys. Rev. B **52**, 1631 (1995).
[83] P. Faure and C. Genestier, X-ray diffraction study of pure plutonium under pressure, J. Nucl. Mater. **385**, 38 (2009).
[84] H. Ledbetter, A. Migliori, J. Betts, S. Harrington, and S. El-Khatib, Zero-temperature bulk modulus of alpha-plutonium, Phys. Rev. B **71**, 172101 (2005).
[85] P. Söderlind, A. Landa, J. E. Klepeis, Y. Suzuki, and A. Migliori, Elastic properties of Pu metal and Pu-Ga alloys, Phys. Rev. B **81**, 224110 (2010).
[86] S. Heathman, R. G. Haire, T. Le Bihan, A. Lindbaum, K. Litfin, Y. Méresse, and H. Libotte, Pressure Induces Major Changes in the Nature of Americium's 5*f* Electrons, Phys. Rev. Lett. **85**, 2961 (2000).
[87] R. Haire, J. Peterson, U. Benedict, C. Dufour, and J. Itié, X-ray diffraction of curium-248 metal under pressures of up to 52 GPa, J. Less Common Metals **109**, 71 (1985).
[88] S. Heathman, R. G. Haire, T. Le Bihan, A. Lindbaum, M. Idiri, P. Normile, S. Li, R. Ahuja, B. Johansson, and G. H. Lander, A high-pressure structure in curium linked to magnetism, Science **309**, 110 (2005).
[89] F. Nilsson, R. Sakuma, and F. Aryasetiawan, *Ab initio* calculations of the hubbard U for the early lanthanides using the constrained random-phase approximation, Phys. Rev. B **88**, 125123 (2013).
[90] B.-C. Shih, T. A. Abtew, X. Yuan, W. Zhang, and P. Zhang, Screened coulomb interactions of localized electrons in transition metals and transition-metal oxides, Phys. Rev. B **86**, 165124 (2012).
[91] T. Gouder, G. van der Laan, A. B. Shick, R. G. Haire, and R. Caciuffo, Electronic structure of elemental curium studied by photoemission, Phys. Rev. B **83**, 125111 (2011).
[92] W. Xie, W. Xiong, C. A. Marianetti, and D. Morgan, Correlation and relativistic effects in U metal and U-Zr alloy: Validation of *ab initio* approaches, Phys. Rev. B **88**, 235128 (2013).
[93] D. van der Marel and G. A. Sawatzky, Electron-electron interaction and localization in d and f transition metals, Phys. Rev. B **37**, 10674 (1988).
[94] W. Xie, C. A. Marianetti, and D. Morgan, Reply to "comment on 'correlation and relativistic effects in u metal and U-Zr alloy: Validation of *ab initio* approaches"', Phys. Rev. B **93**, 157101 (2016).
[95] P. Söderlind, A. Landa, and P. E. A. Turchi, Comment on "correlation and relativistic effects in U metal and U-Zr alloy: Validation of *ab initio* approaches", Phys. Rev. B **90**, 157101 (2014).
[96] W. Xie, C. A. Marianetti, and D. Morgan, Applicability of DFT + U to U metal and U-Zr alloy, arXiv:1601.07959 [cond-mat.mtrl-sci].
[97] P. Söderlind, Ambient pressure phase diagram of plutonium: A unified theory for α-Pu and δ-Pu, Europhys. Lett. **55**, 525 (2001).
[98] P. Söderlind, Quantifying the importance of orbital over spin correlations in δ-Pu within density-functional theory, Phys. Rev. B **77**, 085101 (2008).
[99] O. J. Wick, *Plutonium Handbook A Guide to the Technology* (Gordon and Breach Science Publishers, New York, 1967).
[100] W. H. Zachariasen, Crystal chemical studies of the 5*f*-series of elements. XVII. the crystal structure of neptunium metal, Acta Crystallographica **5**, 660 (1952).
[101] S. Dabos, C. Dufour, U. Benedict, and M. Pagès, Bulk modulus and p- v relationship up to 52 gpa of neptunium metal at room temperature, J. Magn. Magn. Mater. **63-64**, 661 (1987).
[102] D. C. Wallace, Electronic and phonon properties of six crystalline phases of Pu metal, Phys. Rev. B **58**, 15433 (1998).
[103] M. D. Jones, J. C. Boettger, R. C. Albers, and D. J. Singh, Theoretical atomic volumes of the light actinides, Phys. Rev. B **61**, 4644 (2000).
[104] J.-P. Julien, J.-X. Zhu, and R. C. Albers, Coulomb correlation in the presence of spin-orbit coupling: Application to plutonium, Phys. Rev. B **77**, 195123 (2008).
[105] A. Koga, N. Kawakami, T. M. Rice, and M. Sigrist, Orbital-Selective Mott Transitions in the Degenerate Hubbard Model, Phys. Rev. Lett. **92**, 216402 (2004).
[106] Y. Baer and J. K. Lang, High-energy spectroscopic study of the occupied and unoccupied 5*f* and valence states in Th and U metals, Phys. Rev. B **21**, 2060 (1980).
[107] J. Naegele, L. Cox, and J. Ward, Photoelectron spectroscopy (UPS/XPS) study of Np_2O_3 formation on the surface of neptunium metal, Inorganica Chimica Acta **139**, 327 (1987).
[108] T. Gouder, L. Havela, F. Wastin, and J. Rebizant, Evidence for the 5*f* localisation in thin Pu layers, Europhys. Lett. **55**, 705 (2001).
[109] J. R. Naegele, L. Manes, J. C. Spirlet, and W. Müller, Localization of 5*f* Electrons in Americium: A Photoemission Study, Phys. Rev. Lett. **52**, 1834 (1984).
[110] A. B. Shick, J. Kolorenč, A. I. Lichtenstein, and L. Havela, Electronic structure and spectral properties of Am, Cm, and Bk: Charge-density self-consistent LDA + HIA calculations in the FP-LAPW basis, Phys. Rev. B **80**, 085106 (2009).